Scene-Based Spectral Response Function Shape Discernibility for the APEX Imaging Spectrometer

Jason Brazile, *Student Member, IEEE*, Robert A. Neville, Karl Staenz,
Daniel Schläpfer, Lixin Sun, and Klaus I. Itten, *Fellow, IEEE*

Abstract—Scene-based spectrometer calibration is becoming increasingly interesting due to the decreasing cost of computing resources as compared with laboratory calibration costs. Three of the most important instrument parameters needed for deriving surface reflectance products are per-band bandwidths, i.e., full-width at half-maximum, band centers, and spectral response function (SRF) shape. Methods for scene-based bandwidth and band center retrieval based on curve matching in the spectral regions near well-known solar and atmospheric absorption features have been investigated with satisfying results. The goal of this work is to establish the feasibility of per-band SRF shape discernibility. To this end, at-sensor radiances in multiple application configurations have been modeled using Moderate-Resolution Atmospheric Transmission (MODTRAN) 4 configured for the currently being built Airborne Prism Experiment (APEX) imaging spectrometer in its unbinned configuration (i.e., optimized for spectral resolution). To establish SRF shape discernment feasibility, per-band MODTRAN 4 spectral "filter response function" files have been generated for five common theoretical shapes using APEX nominal bandwidth and band center specifications and are provided as MODTRAN 4 input for the instrument model. In several application configurations, the typically used Gaussian SRF is used as reference and compared with radiances resulting from hypothetical instruments based on the four other shapes to detect differences in selected spectral subsets or "windows" near well-known Fraunhofer features. A relative root-mean-square metric is used to show that discernment in some cases is directly feasible, and in others, feasible if noise reduction techniques (e.g., along-track averaging of homogeneous targets) are possible.

Index Terms—Airborne Prism Experiment (APEX), calibration, hyperspectral, MODTRAN.

I. INTRODUCTION

FOR MANY Earth observation applications, remotely sensed spectral imagery is only useful after the derivation of surface reflectance from a given airborne or spaceborne instrument's radiance measurements. The atmospheric correction involved in this derivation is delicate and greatly affects the accuracy of the resulting spectral reflectance data [4]. Often, additional postprocessing techniques such as spectral smoothing, i.e., spectral polishing [5], or spatial averaging are used (if possible due to target homogeneity) to improve spectral accuracy at the cost of spatial resolution.

However, investigations have shown that it is possible to improve the original derivation of surface reflectance by improving the accuracy of the instrument characteristics given as input to this process [2].

Among instrument parameters used as input for this calculation are detector bandwidths [given as full-width at half-maximum (FWHM)] and band centers. Typically, the values fed as input are those that were determined based on the most recent (or prelaunch) laboratory calibration of the instrument (e.g., via monochromator [6], etalon [7], or low-pressure gas lamps [8]). However, Gao *et al.* [9] introduced and later enhanced [1] an atmospheric/solar feature curve-fitting technique that allows for the refinement of band centers derived from a particular scene recorded by the instrument. Ramon *et al.* [10] and Casadio and Colagrande [11] performed similar Medium-Resolution Imaging Spectrometer (MERIS) calibration based on the O_2 absorption feature. Neville *et al.* [2] also used a feature-based method that is additionally able to refine bandwidth information and further showed that the improvement in resulting surface reflectance can remove the need for additional spectral smoothing. While the accuracy of these feature-matching techniques rely on the correctness of Moderate-Resolution Atmospheric Transmission (MODTRAN) 4 (version 3, revision 1) [12] and its High-Resolution Transmission Molecular Absorption (HITRAN)-based [13] feature database, so does the atmospheric correction of the scene in general—any underlying inaccuracies would anyway negatively affect the derived surface reflectance.

While accurate band center and bandwidth data are assumed to be the most important of the instrument input characteristics in the surface reflectance derivation process, an additional parameter that can be given is the per-band SRF shapes—in place of the standard practice of assuming strictly Gaussian shapes.

The goal of this work is to establish the feasibility of retrieving certain per-band SRF shapes directly from a scene by measuring the effect of notable hypothetical SRFs on radiances modeled under typical situations. The example instrument chosen for this study is the currently being built Airborne Prism Experiment (APEX) imaging spectrometer developed within the framework of the European Space Agency's funding scheme Programme for the Development of Scientific Experiments (PRODEX). The aim of APEX is to present an Earth observation platform that enables the reproducible measurement of the radiance field of the terrestrial surface at a local and regional scale as well as acting as simulator, calibrator, and

target refl.	0.05, 0.1, 0.2, 0.4, 0.8
aerosol model	rural extinction
visibility	5 km, 23 km, 100 km
atmos. model	mid-latitude summer
surface alt.	400 m
sensor alt.	5 km
solar zenith angle	180°
scattering alg.	DISORT (16 iterations)
solar data	Thuillier 2002 [16]
filter resp. func.	Gaussian, Bartlett, cosine, Welch, box [17]

validation experiment fostering imaging spectroscopy application development [3], [14], [15].

II. METHOD

To establish discernment feasibility for typical applications, a range of model parameters were selected to cover multiple target types and multiple aerosol visibilities. To allow the simplification of studying a single surface and target altitude, only Fraunhofer lines were used as the basis for selecting comparative feature windows (i.e., radiance values for bands on either side of a particular feature). Windows surrounding atmospheric (as opposed to solar) features should also be feasible, but results are suspected to be more susceptible to scene-based variation (e.g., in sensor altitude and water vapor content). Selected MODTRAN 4 input parameters are shown in Table I.

Feature windows for comparison of the 75 MODTRAN 4 cases (five target reflectances × three visibilities × five SRF shapes) were selected from among the Fraunhofer lines with prominent enough features determined to be useful with current instruments [18]. For each candidate feature, all window sizes ranging from two to five bands on each side of the feature were iteratively evaluated to choose the "best" window. The window size is then fixed for that particular feature. Iterative window selection allows for tuning the selection of features most suitable for a particular instrument.

Reference filter response functions were arbitrarily selected from standard theoretical models [17] and generated by a MATLAB-based implementation [19] at fixed nominal band centers and FWHMs specified for the APEX instrument. The Gaussian shape of SRF filter generator was verified by both reproducing exactly the example `DATA/aviris.flt` AVIRIS filter response file delivered with MODTRAN 4 [20] for use as the `CARD 1A3 FLTNAM` parameter and measurement via an independently developed Gaussian fitting routine [21].

The Bartlett and box functions were chosen for being extreme cases, and the cosine and Welch functions were chosen for being similar to each other to estimate discernment sensitivity. The chosen evaluation metric for discernment is a relative root mean square (rms) calculated as follows for a Gaussian-based window of radiances, L_G, and a second SRF-based window, L_X:

$$\text{relative rms } (\%) = \frac{\sqrt{\frac{\sum_{i=1}^{n}(L_{Gi}-L_{Xi})^2}{n}}}{\overline{L_{Gi}}} \times 100.$$

This metric has the merit of directly implying nominal[1] signal-to-noise ratio (SNR) values (i.e., SNR = 100/ relative rms) needed by an instrument to achieve discernment, although in practical application, other metrics may have more desirable qualities.

III. RESULTS

The results are visualized in Fig. 1 (for simplicity, at only one of the three visibility values), but the implied nominal instrument SNR requirements for all measurements are shown in Table II.

In the figure, the top row shows six of the well-performing Fraunhofer feature windows (for simplicity, the four candidate SRF-convolved spectra are plotted only at the highest target reflectance of 0.8, whereas the internal plots refer to the entire range), whereas the left column shows the four SRFs that were compared against the standard Gaussian SRF. The internal plots then show the relative rms at five target reflectances (0.05, 0.1, 0.2, 0.4, and 0.8) for the corresponding feature window and SRF.

In Table II, the information in the rows and columns correspond to the same information in the figure, with the addition of the extravisibility dimension (5, 23, and 100 km). Table entries that do not differ from the one directly above it are denoted with *ditto*.

The most interesting general observations of the results are as follows: The Bartlett SRF is generally the least discernible from the Gaussian SRF; the $A(O_2)$ and $B(O_2)$ features seem to have the lowest SNR requirements for discernment; the seemingly very similar cosine and Welch SRFs appear to be easily discernible when compared against the Gaussian; differing visibility and target reflectance values have mostly minor influences on discernibility; for the APEX instrument, most of the best performing feature windows contained only four bands (although some features not shown here did best with five and one with eight bands); and most importantly, SNR requirements for discernment in some cases lie directly within current typical instrument specifications (i.e., without the need to employ signal enhancement postprocessing).

IV. DISCUSSION

When selecting theoretical SRFs for this study, it was assumed that the cosine and Welch functions would most closely match the Gaussian, due to visual inspection of their shape. Inasmuch as the Bartlett function matches the Gaussian the most and the box the least, the spectral coverage of the tails of the SRF has proven to be more important for the resulting signal than the area under the curve above the FWHM. Equally surprising was the ease of discernibility between the cosine and Welch functions with respect to the Gaussian-convolved result. This could also be a result of the same effect, i.e., although their shapes are similar, the coverage of their tails are clearly different.

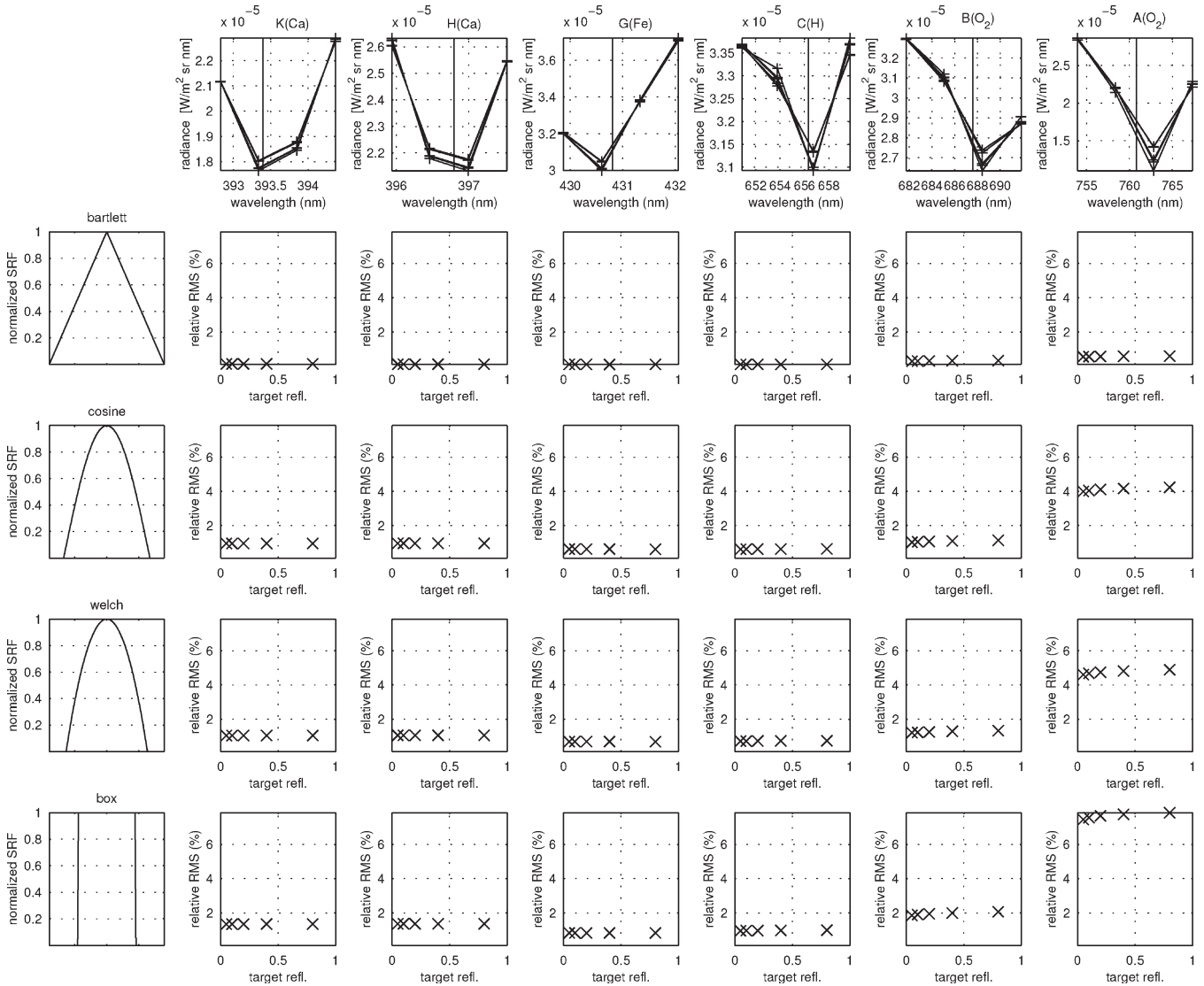[1]A sensor-specific noise model is not addressed in this work.

Fig. 1.   RMS (relative to Gaussian) of radiances for varying target reflectance per SRF per solar feature for selected cases at 5-km visibility.

Unsurprisingly, the good results obtained from the $A(O_2)$ and $B(O_2)$ features validate the popularity of these choices for feature-based calibration in the prevailing literature.

It was unknown what effect differing visibility and target reflectance cases would have on SRF discernibility; thus, the resulting relative invariance shown by the results to these variations have good implications on the simplicity of possible retrieval methods.

Also unpredicted beforehand were the optimal spectral ranges of the feature windows. Inasmuch as most of them (18 out of 21 analyzed) performed best with the smallest window size—two bands on each side of the window—one can be somewhat confident that the resulting differences were most influenced by the features in question, rather than neighboring features or unknown sources.

The most satisfying results are the implied SNR requirements. None of the SRFs required an SNR of more than $1000:1$, and most applications (e.g., snow, agriculture, and mining) deal with target scenes that contain large enough homogeneous areas that along-track averaging can be used to easily achieve this performance.

There are, however, a few questions raised by seemingly anomalous results in Table II. The most interesting, from a shape discernment point of view, arises from the $A(O_2)$ column. Why is it that SRF shape discernment is affected both by allowing visibility to vary (up to 8% between the 5- and 100-km extremes at 0.8 target reflectance) and allowing reflectance to vary (up to 6% between the 0.05 and 0.8 extremes at 5-km visibility), but only in the Bartlett case and not for any of the other shapes? To investigate this, the full-resolution MODTRAN 4 (i.e., `tape7`) output was consulted. As expected, for every group of five cases where the only varying input parameter was the SRF filter, the full-resolution `tape7` files were identical—only the channel-specific postconvolution `channels.out` files differed. Thus, for any of these cases, if the comparative difference between Gaussian-convolved spectra is greater for one shape than it is for another, then it can only be due to either the MODTRAN 4 implementation of this

TABLE II
INSTRUMENT SNR REQUIREMENTS IMPLIED FROM RELATIVE RMS BETWEEN CANDIDATE SHAPE AND GAUSSIAN (SEE FIG. 1)

feature		K(Ca)			H(Ca)			G(Fe)			C(H)			B(O_2)			A(O_2)			mean
visibility (km)		5	23	100	5	23	100	5	23	100	5	23	100	5	23	100	5	23	100	
	0.05	778	778	778	849	849	849	992	992	992	957	960	959	347	378	395	180	187	189	
	0.1	do.	do.	do.	do.	do.	do.	993	do.	993	951	952	953	338	368	387	178	184	186	
bartlett	0.2	do.	do.	do.	do.	do.	848	do.	993	do.	943	945	948	329	360	381	175	182	185	684
	0.4	do.	do.	do.	do.	do.	do.	994	994	do.	935	939	943	320	352	375	172	180	184	
	0.8	do.	do.	do.	do.	848	do.	do.	do.	do.	923	929	936	308	342	367	170	178	183	
	0.05	105	105	105	104	104	104	161	161	161	162	162	162	97	108	114	25	25	25	
	0.1	do.	do.	do.	do.	do.	do.	do.	do.	do.	161	161	do.	95	105	112	do.	do.	do.	
cosine	0.2	do.	do.	do.	do.	do.	do.	do.	do.	do.	160	do.	161	93	103	111	24	do.	do.	110
	0.4	do.	do.	do.	do.	do.	do.	do.	do.	do.	159	160	do.	91	102	109	do.	do.	do.	
	0.8	do.	do.	do.	do.	do.	do.	do.	do.	do.	158	159	160	88	99	107	do.	24	do.	
	0.05	95	95	95	95	95	95	146	146	146	140	141	141	83	92	97	22	22	22	
	0.1	do.	do.	do.	do.	do.	do.	do.	do.	do.	139	140	140	81	90	96	21	do.	do.	
welch	0.2	do.	do.	do.	do.	do.	do.	do.	do.	do.	do.	139	do.	80	88	94	do.	21	do.	97
	0.4	do.	do.	do.	do.	do.	do.	do.	do.	do.	138	138	139	78	87	93	do.	do.	do.	
	0.8	do.	do.	do.	do.	do.	do.	do.	do.	do.	136	137	138	75	84	91	20	do.	21	
	0.05	74	74	74	73	73	73	121	121	121	105	106	106	54	60	63	13	14	14	
	0.1	do.	do.	do.	do.	do.	do.	do.	do.	do.	do.	105	105	53	58	62	do.	13	13	
box	0.2	do.	do.	do.	do.	do.	do.	122	122	122	104	104	do.	52	57	61	do.	do.	do.	74
	0.4	do.	do.	do.	do.	do.	do.	do.	do.	do.	103	do.	104	50	56	60	do.	do.	do.	
	0.8	do.	do.	do.	do.	do.	do.	do.	do.	do.	102	103	do.	49	54	59	do.	do.	do.	
mean			263			280			355			337			151			60		

convolution or, more likely, simply a data-dependent mathematical artifact of either the convolution or the use of the relative rms as the spectra discernment metric.

Finally, how can it be that for features K(Ca), H(Ca), and G(Fe), relative discernibility between SRF shapes is unaffected when visibility and target reflectance are allowed to vary, yet in the case of the B(O_2) feature at 5-km visibility, Bartlett shape discernibility differed by 13% when reflectance was allowed to vary between the 0.05 and 0.8 extremes? Again, this outcome is directly due to the results produced by the underlying MODTRAN 4 [12] and HITRAN [13] models and are beyond the scope of this letter. However, we feel that a maximum deviation in SNR of 13% for a 1600% change in reflectance does not present a major hurdle in the development of a useful SRF shape retrieval algorithm.

V. CONCLUSION

The discernibility of the four theoretical SRFs from the typically used Gaussian and their respective SNR requirements at various Fraunhofer feature windows has been shown for an instrument modeled on the currently being built APEX [3] imaging spectrometer.

For some feature windows, these SNR values are already within specification of current typical instruments such as APEX. For other feature windows, the required SNR can often be achieved with signal enhancement techniques such as along-track averaging of homogeneous targets.

It is suggested that because two of the examined SRFs were so similar, sensitivity of discernment may yield retrieval of realistic SRFs within a useful resolution. Additionally, iterative feature window analysis allows for tuning the selection of features that are most suitable for a particular instrument.

Ultimately, a band-by-band SRF retrieval method would involve finding as many useful features as possible over an instrument's entire spectral range. It is suggested that in addition to the Fraunhofer features shown here, atmospheric feature windows could be used for this purpose, but their use is more susceptible to per-scene variation [22], which adds more complexity to such a method. Finally, to cover those bands that cannot be retrieved directly via Fraunhofer or atmospheric features, per-detector interpolated fitting would be needed.

A spectrum matching-based SRF retrieval method would minimally use a program such as [19], together with a particular instrument's band center and bandwidth characteristics to pregenerate MODTRAN 4 inputs for a slowly varying lookup table of radiances, indexed by parameterized SRF shapes. Spectrum matching would be performed using some to-be-determined appropriate metric, and retrieval of the shape could be performed by reverse mapping the best matching lookup table entry index to its shape. If the parameterized shapes chosen have appropriate characteristics (e.g., continuity), iterative searching might be possible for increasing the accuracy of the retrieved shape. In any case, a shape retrieval method would need to be integrated with band center and bandwidth retrieval methods, as these iterative matching methods are not likely to be strictly independent.

Finally, to compliment investigation on SRF retrieval methods, it is recommended to perform a sensitivity study on the effects of using incorrect SRF shapes in surface reflectance product generation to ensure that such a retrieval is practically worthwhile.

REFERENCES

[1] B.-C. Gao, M. J. Montes, and C. O. Davis, "Refinement of wavelength calibrations of hyperspectral imaging data using a spectrum-matching technique," *Remote Sens. Environ.*, vol. 90, no. 4, pp. 424–433, Apr. 2004.

[2] R. A. Neville, L. Sun, and K. Staenz, "Detection of spectral line curvature in imaging spectrometer data," in *Proc. SPIE—Algorithms and Technologies for Multispectral Hyperspectral and Ultraspectral Imagery IX*, S. Shen and P. Lewis, Eds., 2003, vol. 5093, pp. 144–154

[3] J. Nieke, K. I. Itten, W. Debryun, and APEX team, "The airborne imaging spectrometer APEX: From concept to realization," *Proc. EARSeL 4th Workshop Imag. Spectrosc.,* Zagojiewski, Ed., Warsaw, Poland, 2005, pp. 67–74.

[4] R. O. Green, "Spectral calibration requirement for Earth-looking imaging spectrometers in the solar-reflected spectrum," *Appl. Opt.*, vol. 37, no. 4, pp. 683–690, Feb. 1998.

[5] J. W. Boardman, "Post-ATREM polishing of AVIRIS apparent reflectance data using EFFORT: A lesson in accuracy versus precision," in *Proc. Summ. 7th JPL Airborne Earth Sci. Workshop*, 1998, vol. JPL Pub. 97-21, p. 53.

[6] T. Cocks, R. Jenssen, A. Stewart, I. Wilson, and T. Shields, "The HyMap(TM) airborne hyperspectral sensor: The system, calibration and performance," in *Proc. 1st EARSEL Workshop Imag. Spectrosc.*, Zurich, Switzerland, 1998, pp. 37–42.

[7] P. Sinclair, R. Berman, C. Hersom, and A. Hollinger, "Spectral calibration of hyperspectral imagers using a white light etalon," in *Proc. 12th CASI Conf. Astronaut.*, 2002.

[8] E. J. Milton and K. Y. Choi, "Estimating the spectral response function of the CASI-2," in *Proc. Annu. Conf. Remote Sens. Photogramm. Soc.*, Sep. 2004.

[9] B.-C. Gao, M. J. Montes, and C. O. Davis, "A curve-fitting technique to improve wavelength calibrations of imaging spectrometer data," in *Proc. 11th JPL Airborne Earth Sci. Workshop*, 2002, vol. JPL Pub. 03-4, pp. 99–105

[10] D. Ramon, R. P. Santer, and P. Dubuisson, "MERIS in-flight spectral calibration in O_2 absorption using surface pressure retrieval," in *Proc. SPIE—Optical Remote Sensing of the Atmosphere and Clouds III*, H.-L. Huang, D. Lu, and Y. Sasano, Eds., Apr. 2003, vol. 4891, pp. 505–514

[11] S. Casadio and P. Colagrande, "Meris O_2 calibration using SCIAMACHY measurements," in *Proc. MERIS User Workshop*, Nov. 2003.

[12] A. Berk, L. Berstein, G. Anderson, P. Acharya, D. Robertson, J. Chetwynd, and S. Adler-Golden, "MODTRAN cloud and multiple scattering upgrades with applications to AVIRIS," *Remote Sens. Environ.*, vol. 65, no. 3, pp. 367–375, 1998.

[13] L. Rothman, A. Barbe, D. C. Benner, L. Brown, C. Camy-Peyret, M. Carleer, K. Chance, C. Clerbaux, V. Dana, V. Devi, A. Fayt, J.-M. Flaud, R. Gamache, A. Goldman, D. Jacquemart, K. Jucks, W. Lafferty, J.-Y. Mandin, S. Massie, V. Nemtchinov, D. Newnham, A. Perrin, C. Rinsland, J. Schroeder, K. Smith, M. Smith, K. Tang, R. Toth, J. V. Auwera, P. Varanasi, and K. Yoshino, "The HITRAN molecular spectroscopic database: Edition of 2000 including updates through 2001," *J. Quant. Spectrosc. Radiat. Transf.*, vol. 82, no. 1–4, pp. 5–44, Nov. 2003.

[14] K. I. Itten, M. Schaepman, L. De Vos, L. Hermans, H. Schläepfer, and F. Droz, "APEX—Airborne prism experiment: A new concept for an airborne imaging spectrometer," in *Proc. 3rd Int. Airborne Remote Sens. Conf. Exhib.*, 1997, vol. 1, pp. 181–188.

[15] M. Schaepman and K. Itten, "APEX—Airborne PRISM experiment: An airborne imaging spectrometer serving as a precursor instrument of the future ESA land surface processes and interactions mission," in *Proc. ISPRS Comm. VII Symp. Resour. Environ. Monit.*, Budapest, Hungary, 1998, vol. 22(7), pp. 31–37.

[16] G. Thuillier, M. Hersé, D. Labs, T. Foujols, W. Peetermans, D. Gillotay, P. C. Simon, and H. Mandel, "The solar spectral irradiance from 200 to 2400 nm as measured by the SOLSPEC spectrometer from the Atlas and Eureca missions," *Sol. Phys.*, vol. 214, no. 1, pp. 1–22, May 2003.

[17] E. W. Weisstein. (2005, Dec.). Full width at half maximum. [Online]. Available:http://mathworld.wolfram.com/FullWidthatHalfMaximum.html

[18] R. A. Nevillein "Spectral absorption features for use in calibrating imaging spectrometers," Canada Centre for Remote Sensing, Ottawa, ON, Canada, Tech. Rep. CHTN_2003_002, 2003.

[19] J. Brazile. (2005). MODTRAN-Compatible SRF Generator. [Online]. Available: http://www.mathworks.com/matlabcentral/fileexchange/loadFile.do?objectId=8723

[20] A. Berk, G. Anderson, P. Acharay, M. Hoke, J. Chetwynd, L. Bernstein, E. Shettle, M. Matthew, and S. Adler-Golden, *MODTRAN 4 Version 3 Revision 1 User's Manual*.   Bedford, MA: Hanscom AFB, 2003.

[21] J. Blake. (2005). Fitgauss. [Online]. Available: http://www.mathworks.com/matlabcentral/fileexchange/loadFile.do?objectId=7489

[22] D. Schläpfer and J. Nieke, "Operational simulation of at sensor radiance sensitivity using the MODO/MODTRAN environment," in *Proc. EARSeL 4th Workshop Imag. Spectrosc.*, Zagojiewski, Ed., Warsaw, Poland, 2005, pp. 611–619.